Bacteriophage SP01 Gene Product 56 (gp56) Inhibits *Bacillus subtilis* Cell Division by Interacting with DivIC/FtsL to Prevent Pbp2B/FtsW Recruitment

Amit Bhambhani[*1], Isabella Iadicicco[*1], Jules Lee[*1], Syed Ahmed[1], Max Belfatto[1], David Held[1], Alexia Marconi[1], Aaron Parks[1], Charles R. Stewart[2], William Margolin[3], Petra Anne Levin[4], and Daniel P. Haeusser[†1]

[*]These undergraduate authors contributed equally to the work

[1]Biology Department, Canisius College, Buffalo, NY, USA. [2]Department of BioSciences, Rice University, Houston, TX, USA. [3]Department of Microbiology and Molecular Genetics, McGovern Medical School, University of Texas, Houston, USA. [4]Department of Biology, Washington University in St. Louis, St. Louis, MO, USA.

[†]Corresponding Author: haeussed@canisius.edu

ABSTRACT

Previous work identified gp56, encoded by the lytic bacteriophage SP01, as responsible for inhibition of *Bacillus subtilis* cell division during its infection. Assembly of the essential tubulin-like protein FtsZ into a ring-shaped structure at the nascent site of cytokinesis determines the timing and position of division in most bacteria. This FtsZ ring serves as a scaffold for recruitment of other proteins into a mature division-competent structure permitting membrane constriction and septal cell wall synthesis. Here we show that expression of the predicted 9.3-kDa gene product 56 (gp56) of SP01 inhibits latter stages of *B. subtilis* cell division without altering FtsZ ring assembly. GFP-tagged gp56 localizes to the membrane at the site of division.

While its localization permits recruitment of early division proteins, gp56 interferes with the recruitment of late division proteins, including Pbp2b and FtsW. Imaging of cells with specific division components deleted or depleted and two-hybrid analysis suggest that gp56 localization and activity depends on its interaction with mid-recruited proteins DivIC and/or FtsL. Together these data support a model where gp56 interacts with a central part of the division machinery to disrupt late recruitment of the division proteins involved in septal cell wall synthesis.

IMPORTANCE

Research over the past decades has uncovered bacteriophage-encoded factors that interfere with host cell shape or cytokinesis during viral infection. Phage factors that cause cell filamentation that have been investigated to date all act by targeting FtsZ, the conserved prokaryotic tubulin homolog that composes the cytokinetic ring in most bacteria and some groups of archaea. However, the mechanism of several identified phage factors that inhibit cytokinesis remain unexplored, including gp56 of bacteriophage SP01 of *Bacillus subtilis*. Here, we show that unlike related published examples of phage inhibition of cyotkinesis, gp56 blocks *B. subtilis* cell division without targeting FtsZ. Rather, it utilizes the assembled FtsZ cytokinetic ring to localize to the division machinery and block recruitment of proteins needed for the septal cell wall synthesis.

INTRODUCTION

Most bacteria initiate cytokinesis through regulated assembly of the conserved tubulin-like GTPase FtsZ at the future site of division. FtsZ assembles into a toroidal array of treadmilling polymers that serve as a platform for recruitment of the cell division machinery, including

47 enzymes needed for septal cell wall synthesis (1). Proper placement of the FtsZ ring in time and
48 space is required to ensure that newborn cells reach adequate size and contain a full genetic
49 complement. To achieve this, FtsZ assembly at mid-cell and subsequent division are highly
50 precise, with less than a 1% margin of error, suggesting a highly regulated process (2, 3).
51 Blocking FtsZ assembly prevents membrane invagination and septal cell wall synthesis, leading
52 to filamentous, multinucleated cells and eventual cell death (4).
53
54 As a conserved protein that is essential for division in most bacteria, FtsZ is an appealing target
55 of study for both physiologically relevant modes of its regulation and for potential development
56 of novel antibiotics (5–7). Included among cellular regulators of FtsZ assembly are proteins
57 encoded in regions of the *E. coli* genome that originally derived from phage, now turned
58 inactive. Cells have co-opted several of these so-called cryptic phage genes for increased host
59 fitness under particular conditions. These include *dicB* and *dicF* of cryptic phage Qin (aka phage
60 Kim) and the *kilR* (*orfE*) gene of cyptic phage Rac (8). The RNA product of *dicF* binds to *ftsZ*
61 mRNA to inhibit its translation (9), while the DicB peptide interacts with FtsZ inhibitor MinC
62 (10) to target ring assembly independently of its normal regulator MinD, but dependent on ZipA
63 (11). Transient division inhibition by cryptic DicB benefits the host by inhibiting phage receptor
64 proteins ManYZ, enhancing immunity to bacteriophage lambda infection by up to 100-fold (12).
65 The KilR peptide of Rac inhibits *E. coli* division through an unknown Min-independent
66 mechanism that also causes increased loss of rod shape (13).
67
68 Functional bacteriophages also appear to encode factors that transiently block host cell division
69 during infection. Expression of the 0.4 gene of T7 phage or *kil* of lambda phage both lead to *E.*

coli cell filamentation through direct interference with FtsZ assembly by their protein products (14–16). In both cases, temporary inhibition of host cytokinesis by the phage prior to host lysis results in a subtle competitive advantage for the virus, although the specific nature of these advantages remains unclear.

Although all of the above factors come from phage that infect *E. coli*, it is likely that cytokinesis serves as a target for phage in the majority of other bacterial species as well. One reported example exists for the model Gram-positive species *Bacillus subtilis* and its lytic bacteriophage SP01, gene *56*, which lies in an operon comprising genes 58 through 56 (17). Expression of gene *56* alone, or in the context of the entire operon, leads to *B. subtilis* filamentation and death (18), but the mechanism behind this inhibition of cytokinesis is unknown.

The players involved in *B. subtilis* cytokinesis share commonalities with those involved in the *E. coli* division machinery, but several distinctions also exist (19, 20). Assembly of FtsZ at the membrane in *B. subtilis* involves interaction with the essential, well-conserved protein, FtsA, and with the non-essential protein, SepF, each of which contain a membrane-targeting sequence (21). The non-essential trans-membrane protein EzrA, an inhibitor of FtsZ assembly at the cell poles (22), also plays a separate role as part of the early division machinery by linking FtsZ indirectly to the membrane (23). Subsequent steps include recruitment of a trio of closely-interacting, membrane-spanning proteins: DivIB, FtsL, and DivIC. While *divIB* is dispensable in *B. subtilis* under laboratory conditions, both *ftsL* and *divIC* are essential for cytokinesis (24–26). Cellular levels of DivIB, FtsL, and DivIC are interdependent, closely linked through targeted proteolysis (27, 28). DivIB, FtsL, and DivIC cooperatively function as a complex to recruit the

transpeptidase Pbp2B and the transglycosylase FtsW, both essential for septal cell wall synthesis (29).

Here, we characterize the activity of SP01 gene product 56 (gp56) in inhibition of *B. subtilis* cell division. We find that unlike all previously identified phage-derived inhibitors of cytokinesis, gp56 inhibits division independent of FtsZ. Instead, gp56 localizes to the *B. subtilis* division machinery in an FtsZ-dependent manner where it inhibits recruitment of later division components needed for septal cell wall synthesis. Our results suggest that localization of gp56 to the site of division involves interactions with essential division components FtsL and/or DivIC, and that disruption of their activity leads to reduced recruitment of Pbp2B and FtsW, resulting in cell filamentation and death.

RESULTS

Single copy, chromosomal expression of SP01 bacteriophage *GENE 56* inhibits *B. subtilis* cell division and sporulation.

The previous report of division inhibition by gp56 utilized a multicopy plasmid, pPW19. To determine if gp56 is sufficient to inhibit division in single copy, we generated a strain, DPH102, in which gene *56* was expressed from a chromosomally encoded, IPTG-induced promoter at the amylase locus of *B. subtilis* strain JH642. Induction of gene *56* in DPH102 resulted in cell filamentation (**Fig. 1A**) similar to that previously reported in the *B. subtilis* CB-10 background using pPW18 (18). Consistent with division inhibition, staining the cell membrane with FM4-64 indicated that filaments were generally aseptate, with the exception of occasional septa at

116 midcell. Such septa often appeared broader and ill-formed, consistent with a division block.
117 Uninduced DPH102 cells were also slightly elongated (**Fig. 1A**), consistent with leaky
118 expression of *gp56*.
119
120 For verification purposes, we additionally repeated published results from plasmid-borne gene *56*
121 expression (18), but in our JH642 background. We transformed JH642 with pAP1 (pPW19 with
122 the entire gene *58-56* operon) or pAP6 (pPW19 with gene *56* alone) to generate DPH176 and
123 DPH3, respectively. As previously reported for the CB-10 background, IPTG induction of the
124 operon, or gene *56* alone, both inhibited JH642 *B. subtilis* cell division indistinguishably, without
125 altering cell growth or DNA replication/segregation (data not shown).
126
127 Serial dilution assays verified the lethality of long-term division inhibition, while also showing
128 the reversibility of short-term division inhibition upon return to growth conditions without
129 continued gene *56* induction (**Fig. 1B**). Spot plating of DPH102 mid-log culture dilutions to LB
130 IPTG agar showed a four- to five-log reduction in long-term growth, both pre-grown in LB or
131 LB IPTG liquid media. However, cells expressing gp56 survived comparably to the wild type
132 parental strain if returned to media without IPTG.
133
134 *B. subtilis* typically grows for ~4 to 5 mass-doublings in the absence of division (*e.g.* in the
135 presence of gp56) before growth plateaus and cells entire a viable but non-culturable state (30).
136 Consistent with the previous gp56 report (18), division inhibition by gp56 did not significantly
137 alter these short-term *B. subtilis* growth rates. Under our growth conditions JH642 had a
138 generation time (T_D) of 29.0 +/- 1.1 minutes. Uninduced DPH102 had a similar T_D of 28.3 +/- 0.5

minutes, while induced DPH102 that express gp56 had a T_D of 30.7 +/- 2.2 minutes. Likewise, DNA staining verified that DNA replication and segregation appeared unaffected in DPH102 +/- IPTG (data not shown), consistent with previous reports of gp56 expression.

B. subtilis is well known for forming highly resistant endospores. A key step in sporulation is formation of an asymmetrically positioned septum that establishes two compartments: the larger mother cell and the small "forespore" (31). To determine if gp56 similarly impacts asymmetric division, we assessed its impact on spore formation. Phase-contrast microscopy of JH642 cells plated to DSM agar showed ~83 – 90% of cells with fully formed phase-bright spores (**Fig. 1C**). Consistent with leaky production of gp56 being sufficient to inhibit asymmetric division, only ~40% in % uninduced DPH102 cells. Only ~18% of DPH102 cells showed signs of a phase-bright spore upon gp56 expression (**Fig. 1C**). Moreover, of that minority, most appeared to be bands of phase brightness rather than the typical round shape of a properly formed spore.

The carboxyl-terminal domain of gp56 is essential for division inhibition

To identify regions of gp56 required for division inhibition, we serially passaged DPH3 (JH642 pAP6) on LB IPTG agar to isolate suppressors that grow in the presence of gp56. Plasmid sequencing revealed the overwhelming majority of such isolates had either promoter mutations or nonsense mutations early in the gene 56 coding sequence. One isolate (gene *56Δ65*), however, contained a nonsense mutation at codon 65 of the gene, truncating the predicted gp56Δ65 product by 15 of 79 residues. Analysis of the primary sequence of gp56 by SMART (32) predicts that residues 37 – 59 form a transmembrane domain, with a highly favored orientation prediction

by TMpred (33)where its amino terminus faces the cytoplasm and its carboxyl-terminus faces extracellularly.

To assess the phenotype of gp56Δ65 comparably to the WT, we sub-cloned the gene *56Δ65* allele from its isolated plasmid (pDH89) and placed it under IPTG-inducible control at the *amyE* locus of JH642 to generate DPH175. As expected, single-copy, chromosomal expression of gp56Δ65 failed to cause cell filamentation (**Fig. 1A**) or lethality (**Fig. 1B**). This suggests that gp56Δ65 has lost its ability to inhibit *B. subtilis* cell division, and implicates the predicted extracellular C-terminus of gp56 as essential for mediating that inhibitory phenotype.

Division inhibition by gp56 is independent of FtsZ ring formation.

Previously characterized bacteriophage division inhibitors function by reducing cellular FtsZ concentrations (*e.g. dicF* (9)) or directly antagonizing its assembly (*e.g.* l *kil* (16, 34)). To determine if the same is the case for gp56, we used immunofluorescence microscopy (IFM) to localize FtsZ in wild type, DPH102, and DPH175 cells in the presence an absence of inducer.

As expected for the JH642 wild type background, the majority of cells displayed a single FtsZ ring at mid-cell (**Fig. 2A**), with an average cell length of 4.1 μm and width of 1.3 μm (**Figs. 2B & 2C**). Similar to wild-type cells, uninduced DPH102 cells likewise contained single, medial FtsZ rings (**Fig. 2A**) with an average cell length of 4.5 μm and width of 1.4 μm (**Figs 2B & 2C**). As expected, expression of gp56 in DPH102 resulted in a division block, increasing average cell length to ~18.6 μm (**Fig. 2B**). The average length measurement of these filaments is likely an

185 underestimate, as many filaments extended past the micrograph field of view. Somewhat
186 surprisingly, we observed regularly spaced FtsZ rings along the length of DPH102 cells cultured
187 in the presence of IPTG (**Fig. 2A**). As expected, almost all DPH175 cells contained a single FtsZ
188 ring at midcell (**Fig 2A**) regardless of gp56Δ65 expression. Additionally, DPH175 fixed cell
189 lengths were not altered by expression of the truncated gp56Δ65 (4.2 and 3.9 μm, respectively)
190 (**Fig 2B**). Uninduced DPH175 cells did have a slightly larger average cell width (1.5 μm)
191 compared to induced conditions (1.3 μm) or that of the other strains. While a statistically
192 significant increase by analysis of variance, it is likely an artifact of the fixation process, as
193 similar changes in width are not observed in live cells.
194
195 Although DPH102 filaments formed by gp56 expression still contain FtsZ rings, it is possible
196 they assemble less efficiently. Calculations of length/ FtsZ ring (LR) ratios in DPH102 filaments
197 compared to cells of normal length allow determination of any alteration in FtsZ ring
198 frequency/stability in the presence of gp56. Un-filamented cells had an average L/R ratio of 4.2.
199 In contrast, filamentous DPH102 cells had an average L/R ratio of 7.2. This suggests that while
200 gp56 does not abolish FtsZ ring assembly, it does somewhat reduce them, likely through
201 prolonged filamentation leading to disassembly of preformed FtsZ rings rather than any
202 reduction in their *de novo* assembly. Regardless, such a modest increase in L/R ratio would not
203 explain the observed extreme filamentation.
204
205 ***gp56* interferes with recruitment of essential late division proteins to the site of division.**
206

Together, the preceding data indicate that gp56 acts to block cell division at a step following FtsZ ring formation. Preventing recruitment of other essential proteins of the division machinery to FtsZ, such as enzymes involved in septal peptidoglycan synthesis, also produces a filamentous cell phenotype. To identify the target of gp56, we assayed recruitment of individual GFP-tagged division components in the JH642 *amyE*::P_{spac}-*56* (DPH102) background, in the absence and presence of IPTG inducer.

Our resulting data indicate that gp56 mediated division inhibition occurs through disruption of late protein localization. Green fluorescent protein (GFP) fusions to relatively early localized division proteins EzrA (DPH111) and DivIB (DPH97) exhibited regular staining patterns in filaments formed from gp56 expression, comparable to cells lacking gp56 (**Fig. 3**). In contrast, DivIVA-GFP (DPH371), one of the last proteins recruited during active septation as new daughter cell poles form, exhibited diffuse cytoplasmic staining in filaments formed from gp56 expression.

We next constructed *gfp*-tagged fusions to *ftsW* and *pbp2b* and cloned these at the amylase locus under xylose control (DPH387 and DPH400, respectively). These strains were then transformed with pPW19 or pAP6 to assess potential gp56 effects on GFP-FtsW (DPH408 and DPH409) or GFP-Pbp2B (DPH414 and DPH415) localization. As later recruited proteins, fewer cells in the population normally contain localized GFP-FtsW or GFP-Pbp2B at any given time, compared to early recruited proteins that remain localized for most of the cell cycle. Nonetheless, in the absence of gp56, visible GFP-FtsW and GFP-Pbp2B bands were apparent at mid-cell in multiple cells within a given field of view. In contrast, in the presence of gp56 no cytoplasmic bands of

GFP-Pbp2B were observed, and the only GFP-FtsW bands visible were less uniform in shape (**Fig. 3**) and frequently overlapped with blebs of improperly formed septal cell wall visible through fluorescent WGA staining (**Fig. 3B**)

The diminished recruitment of GFP-FtsW and GFP-Pbp2B by gp56 suggested that the phage peptide might interfere with formation of the DivIB-FtsL-DivIC complex, which cooperatively recruit FtsW and Pbp2B for cell wall septum formation (29). To test this possibility, we constructed *gfp*-tagged fusions to *ftsL* and *divIC* and inserted them at the amylase locus under xylose control (DPH579 and DPH614, respectively). These strains were then transformed with pPW19 or pAP6 to assess potential gp56 effects on GFP-FtsL (DPH1108 and DPH584) or GFP-DivIC (DPH617 and DPH618) localization.

Upon their induction, both GFP-FtsL and GFP-DivIC each demonstrated localization to mid-cell in the absence of gp56, as expected. Additionally, GFP-FtsL and GFP-DivIC still were capable of localizing as cytoplasmic bands within cell filaments formed from gp56 expression. However, this localization of FtsL and DivIC appeared reduced in the presence of gp56, compared to its absence, and FtsL in particular showed a striking occasional pattern of disrupted localization in helices or blobs (**Fig. 3**).

gp56 co-localizes with the division machinery in a manner that requires FtsZ, FtsA, as well as DivIC and/or FtsL

An inhibitor of bacterial cell division that acts after FtsZ ring assembly might localize to midcell via interactions with components of the division machinery to prevent recruitment of relatively

later components. To determine if this is true for gp56 and the observed loss of FtsW and Pbp2B recruitment in its presence, we constructed a chromosomal fusion of *gfp* to gene *56* at the *amyE* locus under control of xylose (DPH50). We chose an N-terminal GFP tag based on the prediction that the C-terminal end of the gp56 peptide would be extracellular and the N-terminal end intracellular. As a control we also constructed a strain with a similar *gfp* fusion to the inactive gene *56Δ65* allele (DPH170).

Induction of *gfp-56* resulted in cells with a clear band of GFP fluorescence at mid-cell, consistent with GFP-gp56 localization to the divisome. In contrast, induction of the inactive truncated gp56 control showed poor to little localization (**Fig. 4A**). Notably, the addition of the GFP tag to the gp56 peptide does seem to interfere with the peptide's activity in blocking cell division, as cells expressing *gfp-56* did not significantly filament.

To determine if gp56 localization was dependent on FtsZ or downstream components of the divisome we transformed the *amyE*::P_{xyl}-*gfp-56* region of the chromosome into strains that contain deletions, or permit depletion, of specific components of the cell division machinery. Depletion of *ftsZ* (DPH504) abolished GFP-gp56 localization to midcell (**Fig. 4B**), confirming that observed GFP-gp56 bands reflect localization to the site of division in a manner requiring the foundational assembled FtsZ.

We next sought to address what other components – if any in addition to FtsZ – were involved in recruitment of gp56 to its site of activity at the divisome. Not surprisingly, depletion of *ftsA* (DPH503) also led to the loss of almost all GFP-gp56 localization. However, deletion of either

276 *divIB* or *ezrA* (DPH55 and DPH177, respectively) did not result in any alteration of GFP-gp56
277 localization compared to that seen in the wild-type background (**Fig. 5**).
278
279 Given these results and the observed loss of Pbp2B and FtsW localization in the presence of
280 gp56, this leaves DivIC and FtsL as potential key factors that may contribute to gp56 recruitment
281 to the divisome. Depletion of *divIC* resulted in a loss of the majority of GFP-gp56 fluorescent
282 bands (**Fig. 5**). Instead, GFP-gp56 signal mostly appeared at the periphery of cells (membrane
283 localization) and to unproductive septal patches that appeared due to the filamentation of cells
284 depleted for *divIC* (**Fig. 5B**). This argues that DivIC does play a significant role in gp56
285 recruitment to the divisome. Likewise, depletion of *ftsL* (DPH1119) led to a loss in GFP-gp56
286 localization (**Fig. 5**). Notably, however, this strain does not allow the depletion of *ftsL* alone, but
287 only in conjunction with *pbpB* (encoding Pbp2B), within the context of the *yllB-ylxA-ftsL-pbpB*
288 operon. Because gp56 appears to prevent Pbp2B localization to the divisome, we would predict
289 that depletion of *pbpB* alone should not lead to any loss of GFP-gp56 recruitment to the
290 divisome. Indeed, following depletion of *pbpB* alone (DPH1121), GFP-gp56 retained its normal
291 localization (**Fig. 5**). This argues that the observed loss of its localization following depletion of
292 *ftsL* and *pbpB* together likely stems from the lack of FtsL specifically.
293
294 **DivIC and FtsL interact with gp56 by bacterial two-hybrid assay.**
295
296 Observed disruptions in normal DivIC and FtsL localization in the presence of gp56, coupled
297 with the observed dependence of gp56 localization on the presence of DivIC and FtsL suggests
298 that these three components might directly interact at the divisome. To test for the potential

299 interactions between these proteins, we cloned *divIC*, *ftsL*, gene *56*, and gene *56Δ65* each into
300 pKT25 and gene *56* into pUT18C for analysis by the bacterial two-hybrid assay (35). We
301 combined each pKT25 construct together with pUT18C-gene *56* in the DHM1 reporter strain and
302 plated the resulting strains to appropriate media. The results of these bacterial two-hybrid
303 analyses indicate that gp56 is capable of strong self-interaction as well as interaction with both
304 FtsL and DivIC. In contrast, interaction with gp56Δ65 is absent (**Fig. 6A**).
305
306 **DivIC overexpression supports the model that gp56 interacts with it to inhibit cell division.**
307
308 The above results are consistent with a model where gp56 localizes to the divisome through
309 interactions with DivIC and/or FtsL (in turn dependent on FtsZ and FtsA). The interaction of
310 DivIC and FtsL with gp56 partially disrupts their normal localization and thereby presumably
311 compromises their normal functions, leading to a loss of Pbp2B and FtsW recruitment and
312 thereby cell filamentation. We hypothesized that if gp56 interactions with DivIC and/or FtsL are
313 disrupting their normal functions, then perhaps overexpression of either of these components
314 would dilute out the inhibitory effects of gp56 and restoring cell division.
315
316 While simultaneous overexpression of *ftsL* and *pbp2B* did not have any effect on gp56 inhibitory
317 activity (data not shown), we found that overexpression of *divIC* through two separate constructs
318 did suppress gp56 inhibition of cell division (**Fig. 6B**). In the first construct, we utilized a strain
319 with an IPTG-inducible second copy of *divIC* at the amylase locus and transformed it with either
320 pPW19 or pAP6. For the resulting strains (DPH660 and DPH661), IPTG addition simultaneously
321 induces overexpression of *divIC* and gene *56* in pAP6. In contrast to the filamentation seen

normally upon gp56 expression from pAP6, no cell filamentation occurred with the simultaneous overexpression of *divIC* (**Fig. 6B**), suggesting that extra DivIC is protective against gp56 activity. For the second construct, we the divIC overexpression background with chromosomal expression of gene *56* from the *thrC* locus through xylose induction (DPH1152). When xylose alone was added to the resulting strain, gp56 expression led to cell filamentation as expected. However, inclusion of IPTG in addition to the xylose allowed *divIC* overexpression and led to rescue from the gp56-mediated block in cell division (**Fig. 6B**). Together these data support the model in which gp56 interferes with DivIC to block further divisome component recruitment, but that additional cellular DivIC can dilute out these effects.

DISCUSSION

The results reported here demonstrate that the inhibition of *B. subtilis* cell division by gp56 of bacteriophage SP01 is exerted downstream of FtsZ ring assembly. FtsZ rings assemble at regular intervals along undivided *B. subtilis* filaments in the presence of gp56, but these rings do not initiate visible constriction or septation. Expression of division components fused to GFP demonstrates that many still localize in the presence of gp56, but that Pbp2B and FtsW recruitment becomes dramatically reduced. Moreover, mid-cell bands of FtsL and DivIC are slightly reduced or disrupted in the presence of gp56. GFP-tagged gp56 demonstrates FtsZ- and FtsA-dependent localization to mid-cell, and its apparent recruitment to the division machinery also requires DivIC and FtsL. Consistent with these results, gp56 shows interaction with itself, FtsL, and DivIC by bacterial two-hybrid analysis, and overexpression of *divIC*, but not *ftsL* can suppress gp56-mediated division inhibition.

345 Together, our results suggest a model (**Fig. 7**) in which gp56 localizes to the division complex in
346 an FtsAZ-dependent manner through interactions with DivIC/FtsL, where its presence interferes
347 with normal DivIB/FtsL/DivIC activity and proper recruitment of Pbp2B and FtsW.
348
349 SP01 gp56 joins an expanding cast of phage-derived factors that inhibit host cytokinesis,
350 including Kil of bacteriophage lambda (16, 34), gp0.4 of bacteriophage T7 (14, 36), and
351 elements of defective prophage like DicB (12) or *dicF* of Qin (9) and Kil of Rac (13). Notably,
352 however, SP01 gp56 represents the first phage factor described to not target FtsZ directly, or
353 indirectly, in its inhibition of cytokinesis. Instead, gp56 has likely evolved to target division
354 machinery maturation by blocking recruitment of septal cell wall synthesis enzymes. A similar
355 mechanism appears to have evolved in *B. subtilis* with the SOS-induced division inhibitor YneA,
356 which likewise blocks cytokinesis downstream of FtsZ ring assembly (37).
357
358 In the case of SP01 gp56, this strategy also allows the bacteriophage to potentially make use of a
359 nonfunctional division machinery foundation for localization of its own factors, at least gp56. A
360 similar case occurs with p1 of *B. subtilis* bacteriophage ϕ29, which localizes to assembled FtsZ
361 at mid-cell to promote phage particle assembly (38). Localization of p1 requires FtsZ, but not
362 Pbp2B, however whether it interacts directly with FtsZ or utilizes another division protein for its
363 localization like gp56 is unknown. Regardless of its precise interactions, ϕ29 p1 recruitment to
364 the division machinery only modestly interferes with *B. subtilis* cytokinesis (38), unlike the total
365 block in division caused by SP01 gp56.
366

Within the SP01 genome, gene *56* is found at the end of an operon with genes *58* and *57* (17, 18), two genes whose products also lack any homologs in databases, and whose function is unknown. It is possible that the products of these other genes colocalize along with gp56 to the FtsZ ring to carry out an activity for SP01 processing together, similar to that seen with ϕ29 p1, that transiently delays cytokinesis sufficiently to prevent division septum formation from interfering with assembling viral particles.

Analogous temporary division blocks also occur within the *B. subtilis* host, such as during the aforementioned YneA-mediated SOS response to permit DNA repair (37), or during the transition of from vegetative growth to sporulation via RefZ activity on FtsZ (39, 40). It also occurs during the DNA recombination events that accompany the developmental stress response of *B. subtilis* natural competence, where the peptide Maf is produced upon DNA uptake, and directly and transiently inhibits FtsZ assembly to permit uninterrupted genome maintenance (41).

The previous study (18) identifying SP01 gp56 as an inhibitor of *B. subtilis* cytokinesis demonstrated that a temporary block in division does occur during the SP01 infective process prior to host cell lysis. However, SP01 lacking gene *56* displays no apparent phenotypic defect in burst size or latency under laboratory conditions (18). It still remains possible, however, that gp56-mediated cytokinetic blocks give subtle competitive advantages to SP01 under particular growth conditions by preventing cells from dividing over phage particles in the process of assembly. Additionally, given that gp56 also interferes with maturation of the asymmetric FtsZ ring formed during sporulation, that developmental pathway may represent a situation where gp56 becomes more important for SP01 infective success.

Beyond the roles for gp56 in SP01 biology, its apparent interactions with FtsL/DivIC make it a potential tool for further study of the role that these proteins play in *B. subtilis* cell division. Normally, loss of Pbp2B or FtsW localization to the division machinery perturbs 'back-recruitment' of the ternary complex of DivIB/FtsL/DivIC, where they too become delocalized (27–29). However, in the presence of gp56, loss of Pbp2B and FtsW does not result in that perturbation, presumably because FtsL/DivIC interactions with gp56 help protect them from delocalization and/or proteolysis, even while rendering them at least partially dysfunctional.

While overexpression of FtsL did not detectably suppress gp56 activity in inhibiting cell division (data not shown), overexpression of DivIC did, suggesting that additional DivIC might titrate out gp56 effects on itself and FtsL, thereby restoring their ability to effectively recruit the enzymes for septal cell wall synthesis. Recent studies from *E. coli* suggest that FtsQ/FtsL/FtsB (homologs of DivIB/FtsL/DivIC, respectively) together help bridge the activity of the earlier recruited FtsA with the later proteins needed for cell wall synthesis and invagination of the Gram-negative outer membrane (42, 43). Even without the outer membrane structure, a similar type of communication between early and late division proteins might be mediated by DivIB/FtsL/DivIC in *B. subtilis*. Consistent with this, we have isolated a spontaneous suppressor of gp56 activity that maps to *ftsA*. Though gp56 still localizes to the site of division in the presence of this FtsA suppressor, it appears that the mutant FtsA is capable of stabilizing DivIB/FtsL/DivIC components sufficiently despite gp56's presence to still permit recruitment of Pbp2B/FtsW, similar to what is seen upon DivIC overexpression (data not shown). Alternatively, by analogy to the stronger recruitment of the key late *E. coli* divisome protein FtsN by hypermorphic alleles of FtsA (44, 45), our FtsA

mutant may be able to bypass the DivIB/FtsL/DivIC requirement for recruitment of Pbp2/FtsW. The characterization of this gp56-resistant *ftsA* mutant allele and further study of the role that genes *58-56* might play in SP01 biology will be the focus of our future studies.

MATERIALS & METHODS

Bacterial Strains and Growth Conditions

All *B. subtilis* and *E. coli* strains used are listed in Table 1. *B. subtilis* strains used for experiments are derivatives of JH642 (46). *E. coli* strain AG1111 (47) was used for plasmid construction/storage and DHM1 (35) was used for bacterial two-hybrid analysis.

Cells were grown in, or on, LB Lennox (1% tryptone, 0.5% yeast extract, 0.5% NaCl, 0.35 K_2HPO_4, pH 7.4) medium (Teknova) at 30°C for temperature sensitive strains under permissive conditions or 37°C for other strains. Sporulation was induced by exhaustion in Difco sporulation medium (DSM). Antibiotic concentrations were as previously described (23, 48). As appropriate, 1 mM Isopropyl-β-D-thiogalactopyranoside (IPTG) (Gold Biotechnology) was used for induction of the P_{spac} promoter or its derivatives, and 0.5% D-(+)-Xylose (Hitech) was used for induction of the P_{xyl} promoter.

For all experiments, overnight cultures of strains were diluted into fresh LB medium and were cultured to mid-exponential growth, monitored by optical density at 600 nm (OD_{600}) with a Hitachi U-1800 spectrophotometer. Cultures were then diluted a second time to an OD_{600} of 0.025 – 0.05 in appropriate experimental conditions. These cultures were then grown to an OD_{600}

435 between 0.4 and 0.6 and harvested for analysis by microscopy, fixation, or plating as described
436 below.
437
438 Plasmid and Strain Construction
439 Cloning and genetic manipulation were performed using standard techniques (49, 50) using
440 naturally competent *B. subtilis* or chemically competent *E. coli* cells. *Pfu* DNA Polymerase (G
441 Biosciences) was used for PCRs in an Eppendorf Mastercycler; standard restriction enzymes and
442 T4 DNA Polymerase (New England Biolabs) were used for cloning. Plasmid DNA was prepared
443 using the Wizard Plus SV Minipreps DNA Purification Kit, PCR and digest reactions were
444 cleaned up using the Wizard SV Gel and PCR Clean-up System, and chromosomal DNA was
445 prepared using the Wizard Genomic DNA Purification Kit (Promega).
446
447 The final versions of all cloning products were sequenced to verify their construction. DNA
448 sequencing was performed by GeneWiz (South Plainfield, NJ), SeqWright (Houston, TX) or
449 PSOMAGEN, Inc (Rockville, MD). DNA bands were visualized using a GelDoc XR Imager
450 (BioRad) and DNA concentrations were estimated with a NanoDrop ND-1000
451 Spectrophotometer (Thermo Scientific).
452
453 All plasmids are listed in Table 2 and oligonucleotides purchased from IDT DNA or Fisher used
454 for their construction are listed in Table 3. Table 2 includes details on which oligonucleotides
455 were used for the cloning of each plasmid new to this study. Table 3 includes details on
456 oligonucleotide sequence, indication of gene targeted for amplification, and restriction site used
457 in the plasmid construction where appropriate. All *E. coli* strains new to this study, as well as *B.*

458 *subtilis* strains DPH2, DPH3, and DPH176, were cloned by transformation with plasmids as
459 indicated in Tables 1 and 2. All of the remaining *B. subtilis* strains new to this study were cloned
460 by transformation with plasmids as indicated in Tables 1 and 2, followed by screening for single
461 or double-crossover into the *B. subtilis* chromosome. Where appropriate, loss of a plasmid
462 backbone following double-crossover was verified by antibiotic counterselection. Successful
463 integrations at *amyE* were verified by iodine staining on starch plates, and testing for threonine
464 auxotrophy was used to verify successful integration at *thrC*. pJL62 (51) was used for conversion
465 of Cm^r $Spec^s$ strains to Cm^s $Spec^r$ ones. Strain PL1119 was created by first cloning *ftsZ* into
466 pUC19 as indicated in Table 2 to create pPL104, followed by sub-cloning into pRDC19 to create
467 pPL106 for transfer into the *B. subtilis* chromosome. pKT25 and pUT186 (35) were used for
468 bacterial two-hybrid experiments (see below.)
469
470 Spot Dilutions
471 As outlined above, cells used for spot dilutions were taken from fresh cultures grown to an OD_{600}
472 between 0.4 and 0.6 under experimental conditions. Ten-fold serial dilutions of these cultures
473 were prepared into fresh LB media (with or without IPTG as appropriate) in a 96-well plate
474 using a multichannel pipette. A flame-sterilized and cooled, metal-pronged tool was then used to
475 replica-plate spots of serially diluted culture onto LB plates with or without IPTG. These plates
476 were then incubated overnight at 37°C and images were scanned using a flatbed scanner and
477 adjusted for brightness/contrast using Adobe Photoshop.
478
479 Cell Fixation, Microscopy, and Analysis

As outlined above, cells used for spot titers were taken from fresh cultures grown to an OD_{600} between 0.4 and 0.6 under experimental conditions and then harvested for fixation or immediate live visualization by DIC microscopy. Prior to microscopy, live cell samples were stained with the vital membrane stain FM4-64 (Molecular Probes). Cell fixation and preparation for immunofluorescence microscopy, including antibodies employed, were done as previously described (22, 23). Images were processed and analyzed for ring frequency and cell width or length (inter-septal distance for chains of *B. subtilis* cells) measurements using the ObjectJ extension (52) of ImageJ (53).

Microscopy was performed using a 100X DIC (or phase for sporulation) objective on either an Olympus BX60 microscope with a Hamamatsu C8484 camera using HC Image software (Hamamatsu), an Olympus BX51 microscope with an OrcaERG camera (Hamamatsu) using Nikon Elements Advanced Research software, or a Nikon Eclipse TE2000-E using Metavue 7.8 12.0 software (Molecular Devices). Images were processed for brightness/contrast and colorization using Adobe Photoshop.

Bacterial Two-Hybrid (BACTH) Assays

For BACTH experiments (35), DivIC, FtsL or gp56/gp56Δ65 were each fused to the carboxy terminus of T25 from *Bordetella pertussis* in pKT25. Additionally, gp56 was fused to the carboxy terminus of T18 from *Bordetella pertussis* in pUT18C. Plasmids were heat-shock transformed sequentially into competent DHM1 cells and grown at 30°C. Strains were patched onto medium containing 50 g/ml X-Gal (5- bromo-4-chloro-3-indolyl-β-D-galactopyranoside; Gold Biotechnology), 1 mM IPTG, and antibiotics. Patches were screened for a color change

503 following 2 days of incubation at 30°C. An image of the plate was taken using a flatbed scanner
504 and adjusted for brightness/contrast using Adobe Photoshop.
505
506 **ACKNOWLEDGEMENTS**
507 We thank Fabrizio Arigoni, Alan Grossman, Frederico Gueiros-Filho, Liz Harry, and Joe
508 Lutkenhaus for the kind gift of strains and plasmids. We thank members of the Department of
509 Microbiology and Molecular Genetics at UT Houston and the members of the Department of
510 Biology at Canisius College for helpful discussions. This research was made possible through
511 NIH funding to WM (GM61074) and PAL (GM127331), Frieberg Visiting Professor of Biology
512 research funding from the Department of Biology, Washington University in St. Louis to DPH,
513 start-up and departmental research funds from Canisius College to DPH, and Canisius Earned
514 Excellence Program (CEEP) undergraduate student research funding to AB, JL, SA, and AM. II
515 received partial support by the Canisius Science Scholars Program, under an NSF S-STEM
516 award (1643649). Author contributions were as follows: Experiments: AB, II, JL, and DPH;
517 Supporting experiments: SA, MB, DH, AM, and AP; Design, Funding, and Resources: CRS,
518 WM, PAL, and DPH; Writing: DPH.
519
520 **REFERENCES**
521 1. Haeusser DP, Margolin W. 2016. Splitsville: structural and functional insights into the
522 dynamic bacterial Z ring. Nat Rev Microbiol 14:305–319.

523 2. Trueba FJ. 1982. On the precision and accuracy achieved by Escherichia coli cells at fission
524 about their middle. Arch Microbiol 131:55–59.

525 3. Yu X-C, Margolin W. 1999. FtsZ ring clusters in min and partition mutants: role of both the
526 Min system and the nucleoid in regulating FtsZ ring localization. Molecular Microbiology
527 32:315–326.

528 4. Du S, Lutkenhaus J. 2019. At the Heart of Bacterial Cytokinesis: The Z Ring. Trends in
529 Microbiology 27:781–791.

530 5. Tripathy S, Sahu SK. 2019. FtsZ inhibitors as a new genera of antibacterial agents.
531 Bioorganic Chemistry 91:103169.

532 6. Hurley KA, Santos TMA, Nepomuceno GM, Huynh V, Shaw JT, Weibel DB. 2016.
533 Targeting the Bacterial Division Protein FtsZ. J Med Chem 59:6975–6998.

534 7. Wang M, Fang C, Ma B, Luo X, Hou Z. 2019. Regulation of cytokinesis: FtsZ and its
535 accessory proteins. Curr Genet.

536 8. Wang X, Kim Y, Ma Q, Hong SH, Pokusaeva K, Sturino JM, Wood TK. 2010. Cryptic
537 prophages help bacteria cope with adverse environments. Nat Commun 1:147.

538 9. Balasubramanian D, Ragunathan PT, Fei J, Vanderpool CK. 2016. A Prophage-Encoded
539 Small RNA Controls Metabolism and Cell Division in Escherichia coli. mSystems 1.

540 10. Rowlett VW, Margolin W. 2015. The Min system and other nucleoid-independent
541 regulators of Z ring positioning. Front Microbiol 6.

542 11. Johnson JE, Lackner LL, Hale CA, Boer PAJ de. 2004. ZipA Is Required for Targeting of
543 DMinC/DicB, but Not DMinC/MinD, Complexes to Septal Ring Assemblies in Escherichia
544 coli. Journal of Bacteriology 186:2418–2429.

12. Ragunathan PT, Vanderpool CK. 2019. Cryptic-Prophage-Encoded Small Protein DicB Protects Escherichia coli from Phage Infection by Inhibiting Inner Membrane Receptor Proteins. Journal of Bacteriology 201.

13. Conter A, Bouché JP, Dassain M. 1996. Identification of a new inhibitor of essential division gene ftsZ as the kil gene of defective prophage Rac. Journal of Bacteriology 178:5100–5104.

14. Kiro R, Molshanski-Mor S, Yosef I, Milam SL, Erickson HP, Qimron U. 2013. Gene product 0.4 increases bacteriophage T7 competitiveness by inhibiting host cell division. PNAS 110:19549–19554.

15. Haeusser DP, Hoashi M, Weaver A, Brown N, Pan J, Sawitzke JA, Thomason LC, Court DL, Margolin W. 2014. The Kil peptide of bacteriophage lambda blocks Escherichia coli cytokinesis via ZipA-dependent inhibition of FtsZ assembly. PLoS Genet 10:e1004217.

16. Hernández-Rocamora VM, Alfonso C, Margolin W, Zorrilla S, Rivas G. 2015. Evidence That Bacteriophage λ Kil Peptide Inhibits Bacterial Cell Division by Disrupting FtsZ Protofilaments and Sequestering Protein Subunits. J Biol Chem 290:20325–20335.

17. Stewart CR, Casjens SR, Cresawn SG, Houtz JM, Smith AL, Ford ME, Peebles CL, Hatfull GF, Hendrix RW, Huang WM, Pedulla ML. 2009. The Genome of Bacillus subtilis Bacteriophage SPO1. Journal of Molecular Biology 388:48–70.

18. Stewart CR, Deery WJ, Egan ESK, Myles B, Petti AA. 2013. The product of SPO1 gene 56 inhibits host cell division during infection of Bacillus subtilis by bacteriophage SPO1. Virology 447:249–253.

566 19. Rowlett VW, Margolin W. 2015. The bacterial divisome: ready for its close-up.
567 Philosophical Transactions of the Royal Society B: Biological Sciences 370:20150028.

568 20. Errington J, Wu LJ. 2017. Cell Cycle Machinery in Bacillus subtilis, p. 67–101. *In* Löwe, J,
569 Amos, LA (eds.), Prokaryotic Cytoskeletons: Filamentous Protein Polymers Active in the
570 Cytoplasm of Bacterial and Archaeal Cells. Springer International Publishing, Cham.

571 21. Duman R, Ishikawa S, Celik I, Strahl H, Ogasawara N, Troc P, Löwe J, Hamoen LW. 2013.
572 Structural and genetic analyses reveal the protein SepF as a new membrane anchor for the Z
573 ring. PNAS 110:E4601–E4610.

574 22. Haeusser DP, Schwartz RL, Smith AM, Oates ME, Levin PA. 2004. EzrA prevents aberrant
575 cell division by modulating assembly of the cytoskeletal protein FtsZ. Mol Microbiol
576 52:801–814.

577 23. Haeusser DP, Garza AC, Buscher AZ, Levin PA. 2007. The Division Inhibitor EzrA
578 Contains a Seven-Residue Patch Required for Maintaining the Dynamic Nature of the
579 Medial FtsZ Ring. Journal of Bacteriology 189:9001–9010.

580 24. Wadsworth KD, Rowland SL, Harry EJ, King GF. 2008. The divisomal protein DivIB
581 contains multiple epitopes that mediate its recruitment to incipient division sites. Molecular
582 Microbiology 67:1143–1155.

583 25. Daniel RA, Harry EJ, Katis VL, Wake RG, Errington J. 1998. Characterization of the
584 essential cell division gene ftsL(yIID) of Bacillus subtilis and its role in the assembly of the
585 division apparatus. Mol Microbiol 29:593–604.

586 26. Katis VL, Harry EJ, Wake RG. 1997. The Bacillus subtilis division protein DivIC is a
587 highly abundant membrane-bound protein that localizes to the division site. Molecular
588 Microbiology 26:1047–1055.

589 27. Daniel RA, Errington J. 2000. Intrinsic instability of the essential cell division protein FtsL
590 of Bacillus subtilis and a role for DivIB protein in FtsL turnover. Molecular Microbiology
591 36:278–289.

592 28. Daniel RA, Noirot-Gros M-F, Noirot P, Errington J. 2006. Multiple Interactions between
593 the Transmembrane Division Proteins of Bacillus subtilis and the Role of FtsL Instability in
594 Divisome Assembly. Journal of Bacteriology 188:7396–7404.

595 29. Gamba P, Hamoen LW, Daniel RA. 2016. Cooperative Recruitment of FtsW to the
596 Division Site of Bacillus subtilis. Front Microbiol 7.

597 30. Arjes HA, Kriel A, Sorto NA, Shaw JT, Wang JD, Levin PA. 2014. Failsafe Mechanisms
598 Couple Division and DNA Replication in Bacteria. Current Biology 24:2149–2155.

599 31. Tan IS, Ramamurthi KS. 2014. Spore formation in Bacillus subtilis. Environmental
600 Microbiology Reports 6:212–225.

601 32. Letunic I, Bork P. 2018. 20 years of the SMART protein domain annotation resource.
602 Nucleic Acids Res 46:D493–D496.

603 33. Ikeda M, Arai M, Okuno T, Shimizu T. 2003. TMPDB: a database of experimentally-
604 characterized transmembrane topologies. Nucleic Acids Res 31:406–409.

605 34. Haeusser DP, Hoashi M, Weaver A, Brown N, Pan J, Sawitzke JA, Thomason LC, Court
606 DL, Margolin W. 2014. The Kil Peptide of Bacteriophage λ Blocks Escherichia coli
607 Cytokinesis via ZipA-Dependent Inhibition of FtsZ Assembly. PLOS Genetics
608 10:e1004217.

609 35. Karimova G, Pidoux J, Ullmann A, Ladant D. 1998. A bacterial two-hybrid system based
610 on a reconstituted signal transduction pathway. PNAS 95:5752–5756.

611 36. Simpkin AJ, Rigden DJ. 2016. GP0.4 from bacteriophage T7: in silico characterisation of
612 its structure and interaction with E. coli FtsZ. BMC Research Notes 9:343.

613 37. Kawai Y, Moriya S, Ogasawara N. 2003. Identification of a protein, YneA, responsible for
614 cell division suppression during the SOS response in Bacillus subtilis. Molecular
615 Microbiology 47:1113–1122.

616 38. Ballesteros-Plaza D, Holguera I, Scheffers D-J, Salas M, Muñoz-Espín D. 2013. Phage ϕ29
617 protein p1 promotes replication by associating with the FtsZ ring of the divisome in
618 Bacillus subtilis. PNAS 110:12313–12318.

619 39. Wagner-Herman JK, Bernard R, Dunne R, Bisson-Filho AW, Kumar K, Nguyen T,
620 Mulcahy L, Koullias J, Gueiros-Filho FJ, Rudner DZ. 2012. RefZ Facilitates the Switch
621 from Medial to Polar Division during Spore Formation in Bacillus subtilis. Journal of
622 Bacteriology 194:4608–4618.

623 40. Brown EE, Miller AK, Krieger IV, Otto RM, Sacchettini JC, Herman JK. 2019. A DNA-
624 Binding Protein Tunes Septum Placement during Bacillus subtilis Sporulation. Journal of
625 Bacteriology 201.

626 41. Briley K, Prepiak P, Dias MJ, Hahn J, Dubnau D. 2011. Maf acts downstream of ComGA
627 to arrest cell division in competent cells of B. subtilis. Molecular Microbiology 81:23–39.

628 42. Tsang M-J, Bernhardt TG. 2015. A role for the FtsQLB complex in cytokinetic ring
629 activation revealed by an ftsL allele that accelerates division. Molecular Microbiology
630 95:925–944.

631 43. Blaauwen T den, Luirink J. 2019. Checks and Balances in Bacterial Cell Division. mBio 10.

632 44. Pichoff S, Du S, Lutkenhaus J. 2018. Disruption of divisome assembly rescued by FtsN–
633 FtsA interaction in Escherichia coli. PNAS 115:E6855–E6862.

634 45. Busiek KK, Eraso JM, Wang Y, Margolin W. 2012. The Early Divisome Protein FtsA
635 Interacts Directly through Its 1c Subdomain with the Cytoplasmic Domain of the Late
636 Divisome Protein FtsN. Journal of Bacteriology 194:1989–2000.

637 46. Perego M, Spiegelman GB, Hoch JA. 1988. Structure of the gene for the transition state
638 regulator, abrB: regulator synthesis is controlled by the spo0A sporulation gene in Bacillus
639 subtilis. Molecular Microbiology 2:689–699.

640 47. Ireton K, Rudner DZ, Siranosian KJ, Grossman AD. 1993. Integration of multiple
641 developmental signals in Bacillus subtilis through the Spo0A transcription factor. Genes
642 Dev 7:283–294.

643 48. Haeusser DP, Rowlett VW, Margolin W. 2015. A mutation in Escherichia coli ftsZ
644 bypasses the requirement for the essential division gene zipA and confers resistance to FtsZ

645 assembly inhibitors by stabilizing protofilament bundling. Molecular Microbiology 97:988–
646 1005.

647 49. Harwood CR, Cutting SM. 1990. Molecular biological methods for Bacillus. Wiley,
648 Chichester; New York.

649 50. Sambrook J, Russell DW. 2001. Molecular cloning: a laboratory manual. Cold Spring
650 Harbor Laboratory Press, Cold Spring Harbor, N.Y.

651 51. LeDeaux JR, Grossman AD. 1995. Isolation and characterization of kinC, a gene that
652 encodes a sensor kinase homologous to the sporulation sensor kinases KinA and KinB in
653 Bacillus subtilis. Journal of Bacteriology 177:166–175.

654 52. van der Ploeg R, Verheul J, Vischer NOE, Alexeeva S, Hoogendoorn E, Postma M,
655 Banzhaf M, Vollmer W, Blaauwen T den. 2013. Colocalization and interaction between
656 elongasome and divisome during a preparative cell division phase in Escherichia coli.
657 Molecular Microbiology 87:1074–1087.

658 53. Schneider CA, Rasband WS, Eliceiri KW. 2012. NIH Image to ImageJ: 25 years of image
659 analysis. Nature Methods 9:671–675.

660 54. Levin PA, Kurtser IG, Grossman AD. 1999. Identification and characterization of a
661 negative regulator of FtsZ ring formation in Bacillus subtilis. PNAS 96:9642–9647.

662 55. Weart RB, Levin PA. 2003. Growth Rate-Dependent Regulation of Medial FtsZ Ring
663 Formation. Journal of Bacteriology 185:2826–2834.

664 56. Beall B, Lutkenhaus J. 1989. Nucleotide sequence and insertional inactivation of a Bacillus
665 subtilis gene that affects cell division, sporulation, and temperature sensitivity. Journal of
666 Bacteriology 171:6821–6834.

667 57. Levin PA, Losick R. 1994. Characterization of a cell division gene from Bacillus subtilis
668 that is required for vegetative and sporulation septum formation. Journal of Bacteriology
669 176:1451–1459.

670 58. Jaacks KJ, Healy J, Losick R, Grossman AD. 1989. Identification and characterization of
671 genes controlled by the sporulation-regulatory gene spo0H in Bacillus subtilis. Journal of
672 Bacteriology 171:4121–4129.

673 59. Fujita M, Losick R. 2002. An investigation into the compartmentalization of the sporulation
674 transcription factor σE in Bacillus subtilis. Molecular Microbiology 43:27–38.

675 60. Wei P, Stewart CR. 1993. A cytotoxic early gene of Bacillus subtilis bacteriophage SPO1.
676 Journal of Bacteriology 175:7887–7900.

677 61. Norrander J, Kempe T, Messing J. 1983. Construction of improved M13 vectors using
678 oligodeoxynucleotide-directed mutagenesis. Gene 26:101–106.

679

680 **FIGURE LEGENDS**

681 Figure 1 – gp56 inhibits *B. subtilis* cell division. (**A**) Representative micrographs of live JH642
682 (WT), DPH102 (*amyE*::*56*), and DPH175 (*amyE*::*56Δ65*) cells from mid-log cultures (see
683 Materials & Methods) grown in LB with or without 1 mM IPTG, as indicated, for induction of
684 chromosomally-placed gene *56* or gene *56Δ65* at the *amyE* locus. Differential interference

685 contrast (DIC) shows cells in brightfield (top row) and FM4-64 fluorescent staining (bottom
686 row) shows cell membrane to differentiate between undivided, individual cell filaments and
687 multiple, chained cells that form in the JH642 background with septal FM4-64 staining. Scale
688 bar = 5 μm. (**B**) Spot titers of strains as in (A) taken from mid-log cultures grown in LB with or
689 without 1mM IPTG, as indicated, and plated to either LB agar (left) or LB + 1mM IPTG agar
690 (right). Dilution factor of spot titers from original cultures indicated on top. (**C**) Representative
691 phase micrographs of JH642 (WT) and DPH102 (*amyE*::*56*) cells grown in Difco Sporulation
692 Media, with or without 1mM IPTG as indicated. Spores appear as phase-bright dots. Scale as in
693 (A). Percent quantification of total cell counts (n) showing a phase-bright spore for each strain is
694 indicated inset.
695
696 Figure 2 –gp56 does not inhibit FtsZ ring assembly in *B. subtilis*. (**A**) Representative false-
697 colored immunofluorescence micrographs of glutaraldehyde/paraformaldehyde-fixed JH642
698 (WT), DPH102 (*amyE*::*56*), and DPH175 (*amyE*::*56Δ65*) cells taken from mid-log cultures with
699 or without 1mM IPTG as indicated. Fluorescent Wheat germ agglutinin (WGA) staining (top
700 row) shows cell wall, αFtsZ (middle row) shows signal from fluorescent-conjugated secondary
701 antibody to primary antibody against FtsZ. Bottom row shows a merge of the WGA and αFtsZ
702 signals. (**B**) Scatter box plots of cell length (μm) quantification (n > 100) of strains from (A).
703 Box borders denote upper and lower quartiles, with horizontal line in box depicting the median
704 and X depicting the mean. Whiskers show upper and lower deviation of data. (**C**) Scatter box
705 plots of cell width (μm) quantification (n > 100) of strains from (A), with data shown as in (B).
706

Figure 3 – gp56 prevents recruitment of late, essential division proteins needed for *B. subtilis* septal cell wall synthesis. (**A**) Representative false-colored fluorescent micrographs of live cells of strains expressing EzrA-GFP (PL847 and DPH111), GFP-DivIB (DPH79 and DPH97), GFP-DivIC (DPH617 and DPH618), GFP-FtsL (DPH1108 and DPH584), GFP-Pbp2B (DPH414 and DPH415), or GFP-FtsW (DPH408 and DPH409) in the absence (left) or presence (right) of gp56. Each field of view includes a DIC image showing cells in brightfield, FM4-64 showing fluorescently stained membranes, and GFP fluorescent signal showing localization of the indicated fusion construct. Scale bar = 5 μm. (**B**) Merged panels, in same scale, of WGA and GFP signal of from (A).

Figure 4 – GFP-gp56 localizes to the *B. subtilis* site of division in an FtsZ-dependent manner. (**A**) Representative false-colored fluorescent micrographs of live DPH50 (*amyE*::*gfp-56*), and DPH170 (*amyE*::*gfp-56Δ65*) cells taken from mid-log cultures with 0.1% xylose present to induce fusion protein expression. GFP signal (top) shows fusion protein localization and FM4-64 fluorescent signal (bottom) shows cell membranes. Scale bar = 5 μm. (**B**) Representative false-colored fluorescent micrographs of live DPH504 (*ftsZ*::*spc xylA*::*tet thrC*::P_{xyl}-*ftsZ amyE*::P_{spac}-*gfp-56*) cells taken from mid-log cultures with 1 mM IPTG present to induce GFP-gp56 in the presence (left) or absence (right) of xylose to express/deplete FtsZ. GFP signal (top) shows GFP-gp56 localization and FM4-64 fluorescent signal (bottom) shows cell membranes. Scale as in (A).

Figure 5 – GFP-gp56 localization to the *B. subtilis* site of division requires DivIC/FtsL. (**A**) Representative false-colored fluorescent micrographs of live cells taken from mid-log cultures

730 containing (left) or missing (right) FtsA (DPH503), EzrA (JH642 or DPH55), DivIB (JH642 or
731 DPH177), DivIC (DPH302), FtsL and Pbp2B in combination (DPH1121), or Pbp2B alone
732 (DPH1119) through deletion/depletion. Each field of view includes a DIC image showing cells
733 in brightfield, FM4-64 showing fluorescently stained membranes, and GFP fluorescent signal
734 showing localization of GFP-gp56. Scale bar = 5 μm. (**B**) Merged panels, in same scale, of WGA
735 and GFP signal of from (A).
736
737 Figure 6 – SP01 gp56 interacts with itself and *B. subtilis* DivIC or FtsL, and its activity is
738 suppressed by *divIC* over-expression. (**A**) Representative patched growth of DHM1 background
739 *E. coli* strains DPH183 (gp56 alone), DPH164 (gp56 and FtsL), DPH165 (gp56 and DivIC),
740 DPH166 (two copies of gp56), and DPH167 (gp56 and gp56Δ65) bacterial two-hybrid strains
741 containing pUT18C-*56* and indicated pKT25 constructs on LB Amp^{100} Kan^{50} agar plates with 1
742 mM IPTG and 50 g/ml X-Gal. (**B**) Representative false-colored fluorescent micrographs of live
743 cells taken from mid-log cultures with DIC (left) showing cells in brightfield and FM4-64 (right)
744 showing fluorescently stained membranes. DPH660 (*amyE*::P_{spac}-*divIC pPW19*) and DPH661
745 (*amyE*::P_{spac}-*divIC pPW19-56*) grown with 1 mM IPTG to overexpress *divIC* and express gene
746 *56* from pPW19 (top two rows). DPH1152 (*amyE*::P_{spac}-*divIC thrC*::P_{xyl}-*56*) grown with 0.1%
747 xylose to express gene *56* in the absence (third row) or presence (bottom row) of 1 mM IPTG to
748 overexpress *divIC*. Scale bar = 5 μm.
749
750 Figure 7 – SP01 gp56 interacts with *B. subtilis* DivIC/FtsL to disrupt the division machinery and
751 prevent recruitment of the Pbps and FtsW that are essential for septal cell wall synthesis. (**A**) In
752 normal conditions the *B. subtilis* division machinery assembles into a cytokinesis-competent

753 apparatus allowing for proper membrane constriction and septal wall synthesis. FtsZ polymers
754 assemble at the membrane through interactions with membrane-associated FtsA, SepF, and
755 EzrA. Stabilized by non-essential ZapA assembled FtsZ and its membrane-associated partners
756 allow recruitment of DivIB/FtsL/DivIC complexes that in turn help recruit Pbp2B and FtsW,
757 while non-essential GpsB and EzrA help recruit Pbp1. (**B**) In the presence of SP01 gp56, the
758 phage peptide interacts with DivIC/FtsL, mildly disrupting their normal localization and thereby
759 preventing the normal recruitment of Pbp2B, FtsW, Pbp1, and other late division proteins (*e.g.*
760 DivIVA, not shown). While lack of this late recruitment would also normally lead to rapid loss
761 of the DivIB/DivIC/FtsL complex, its interaction with gp56 prevents their loss, effectively
762 freezing the division machinery at a mid-assembled state unable to constrict or build septal cell
763 wall, thereby leading to cell filamentation and death. Cartoon models generated through
764 Biorender.

Figure 1

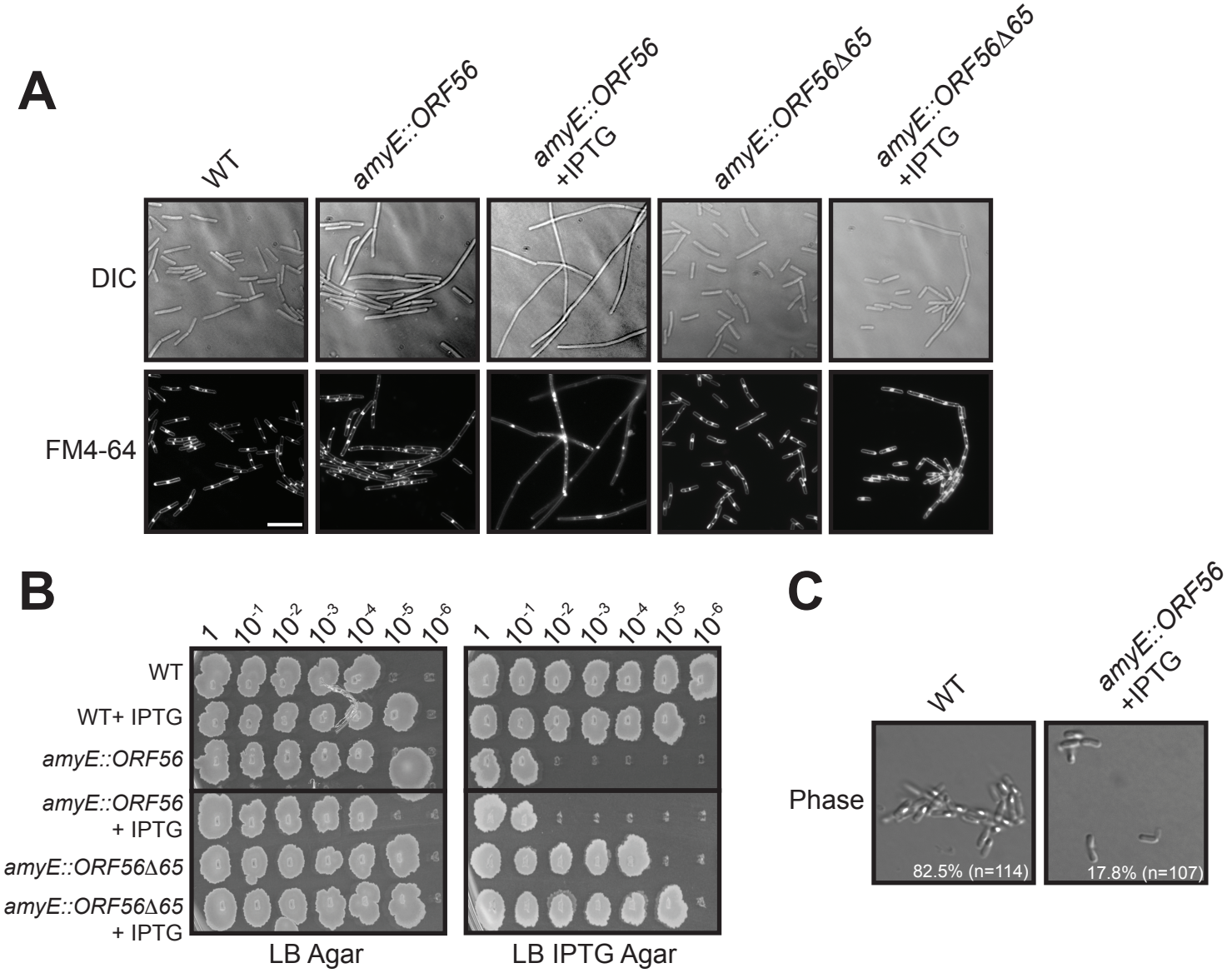

Figure 2

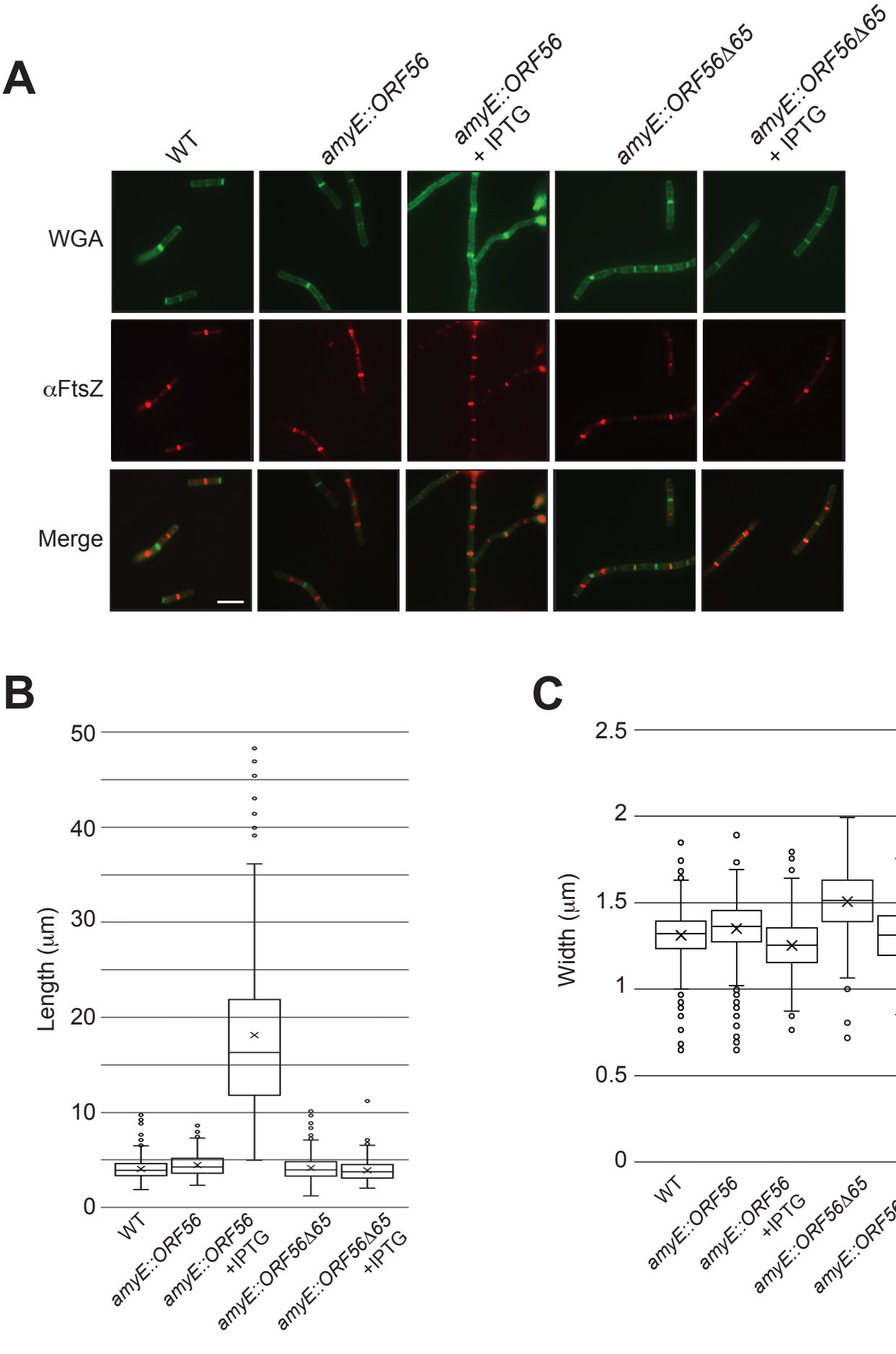

Figure 3

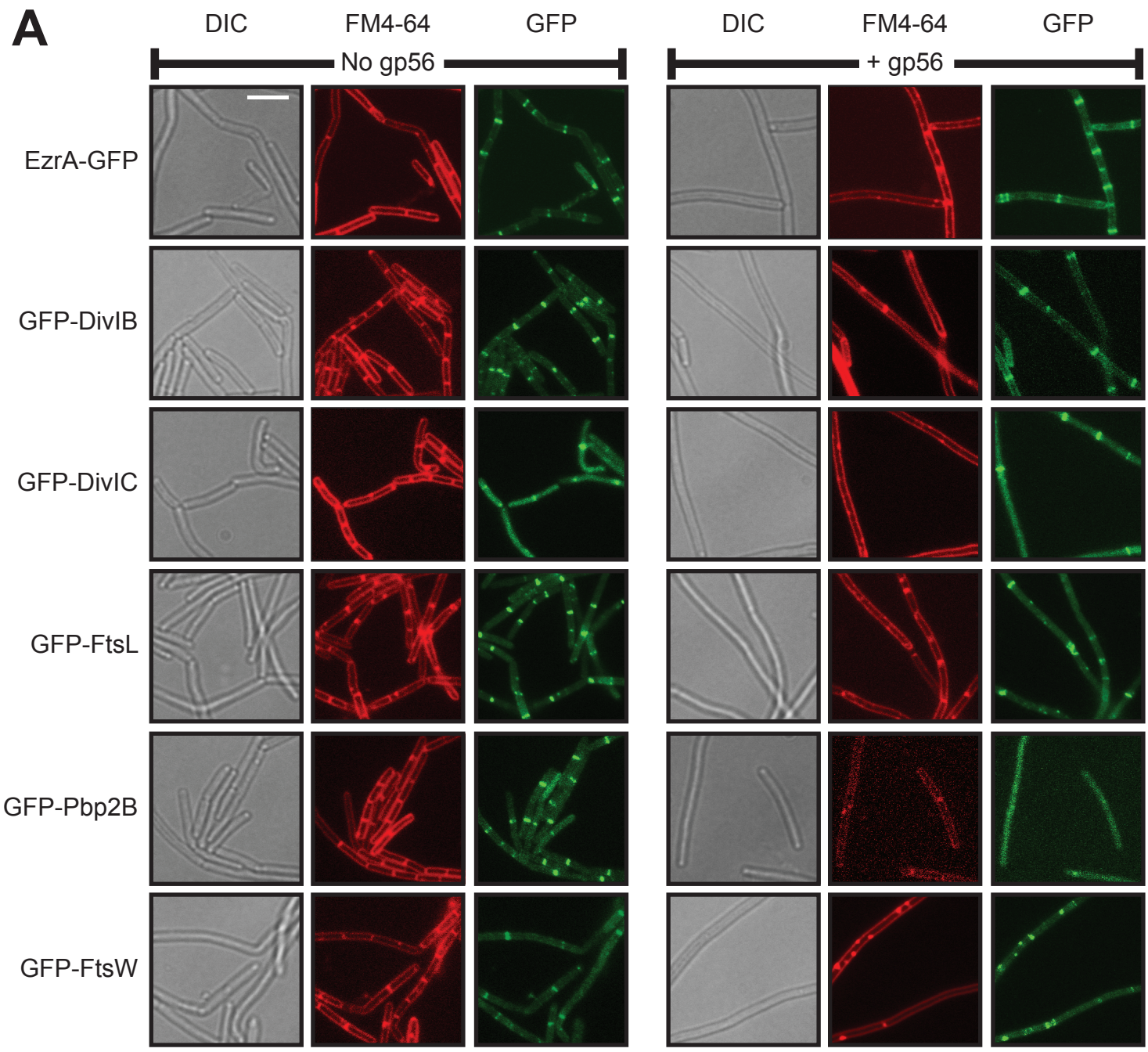

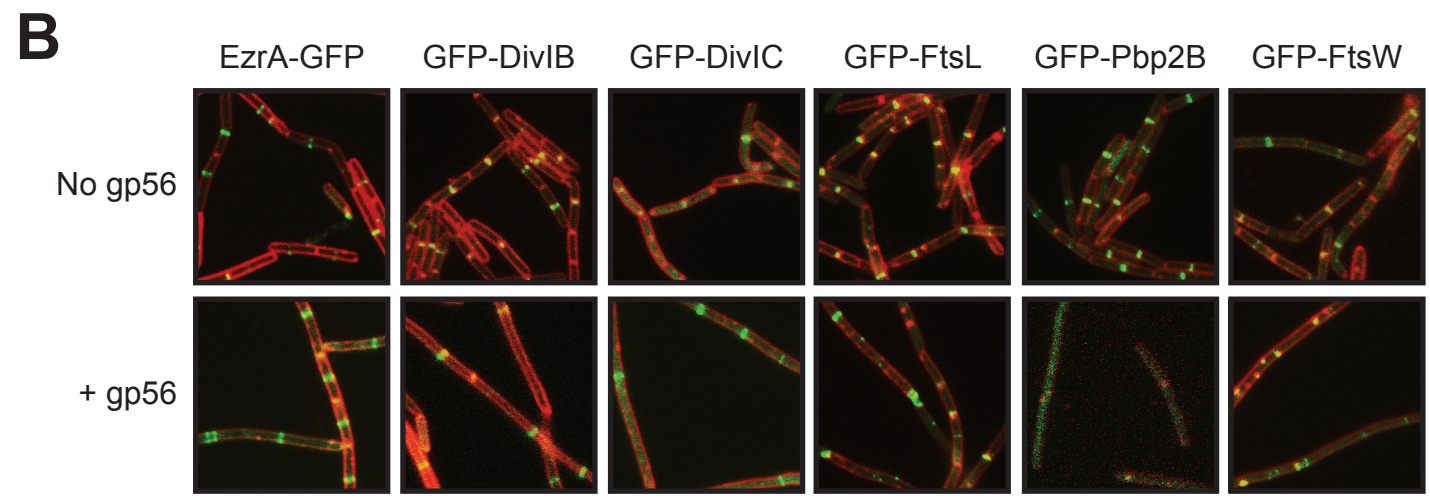

Figure 4

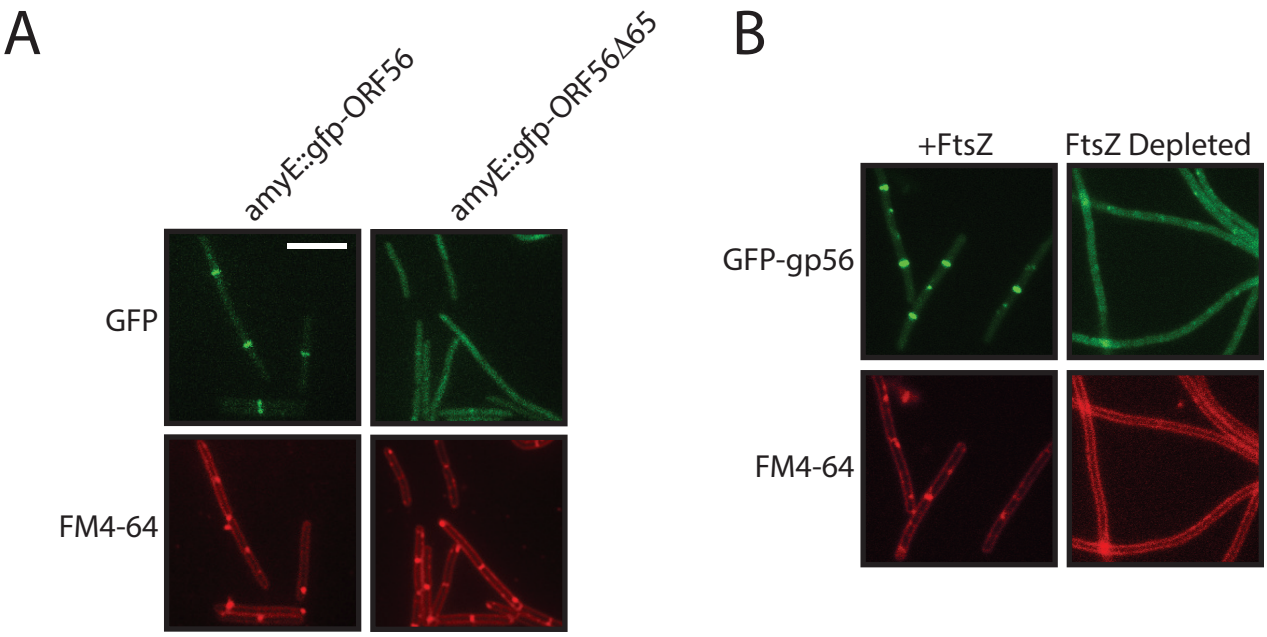

Figure 5

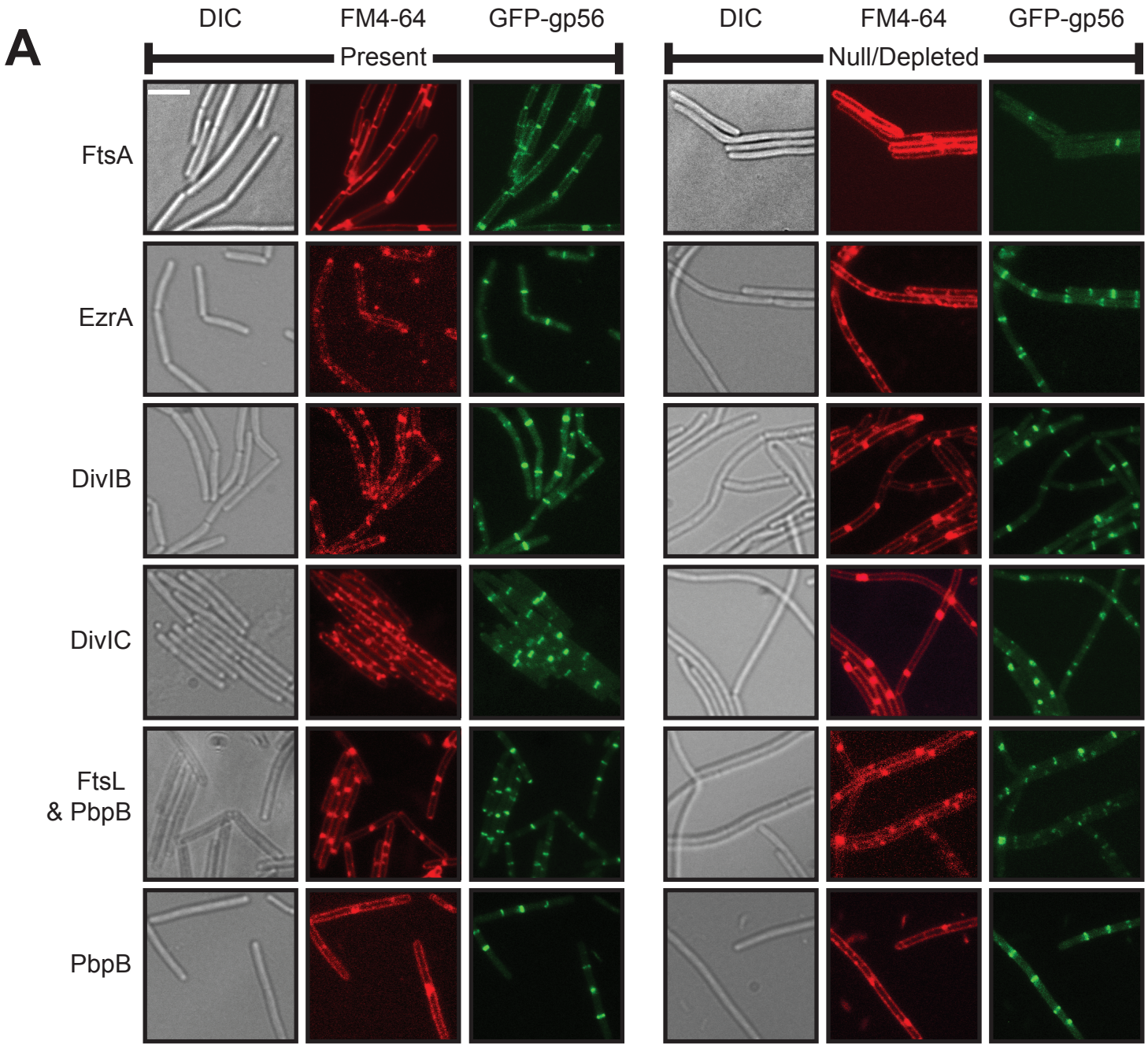

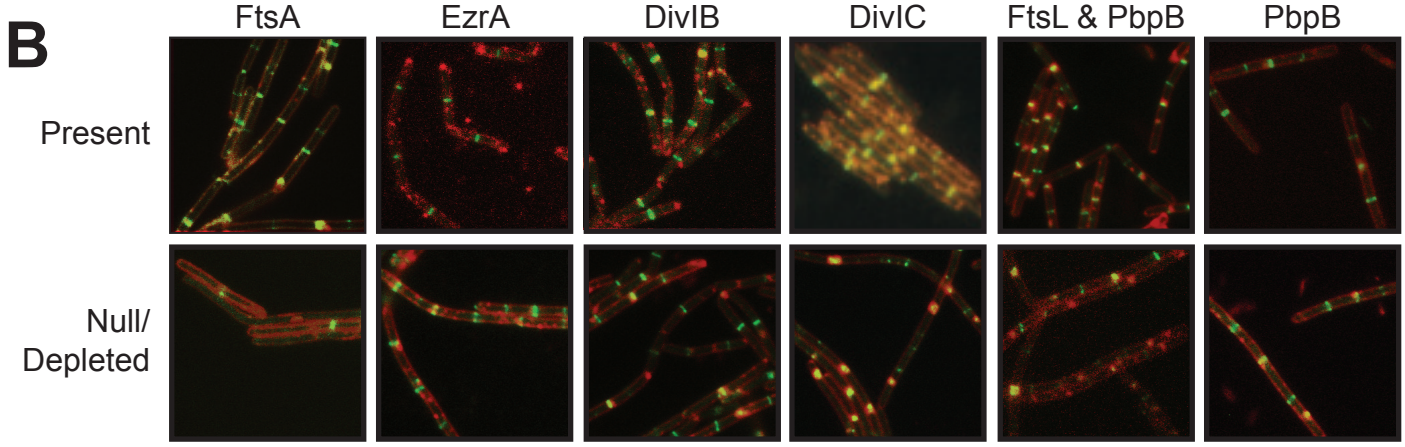

Figure 6

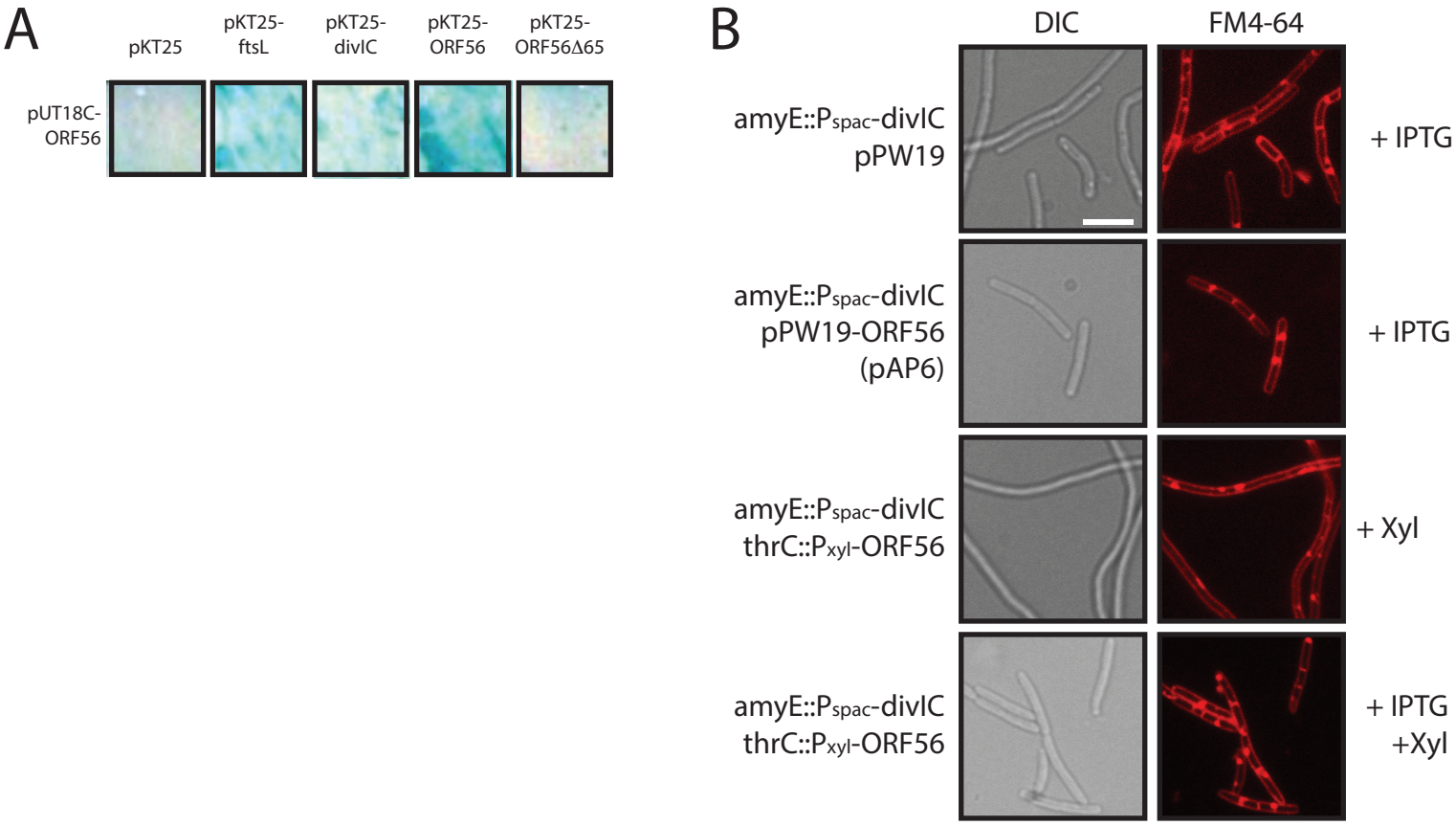

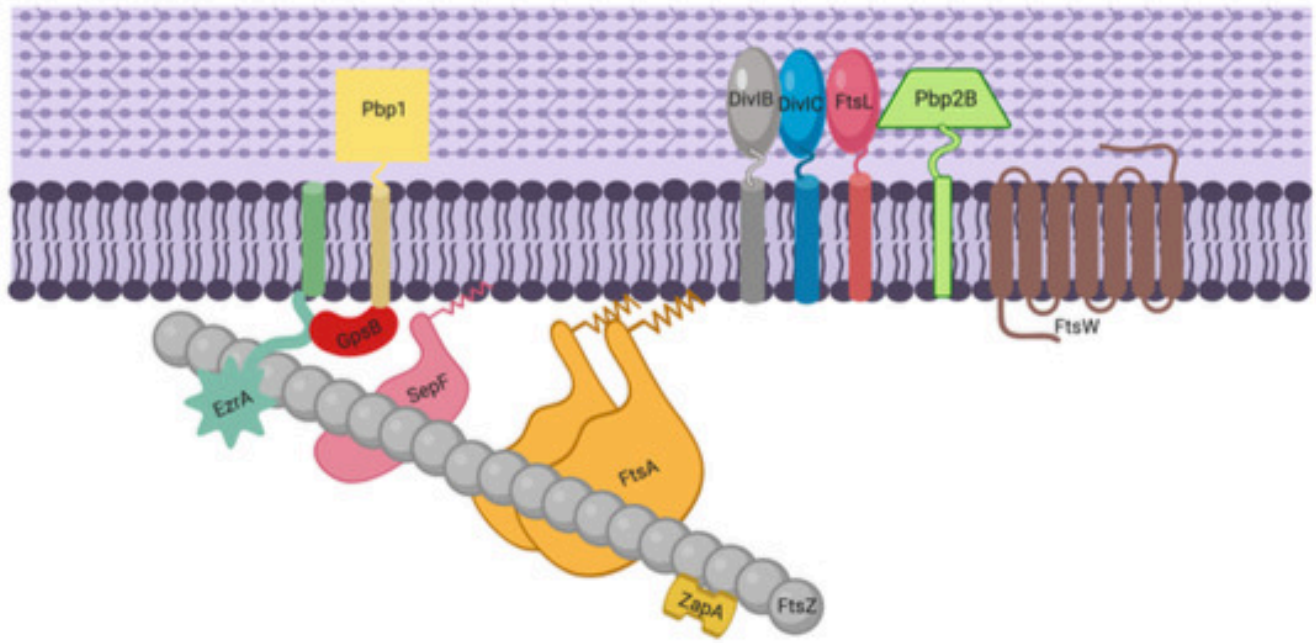

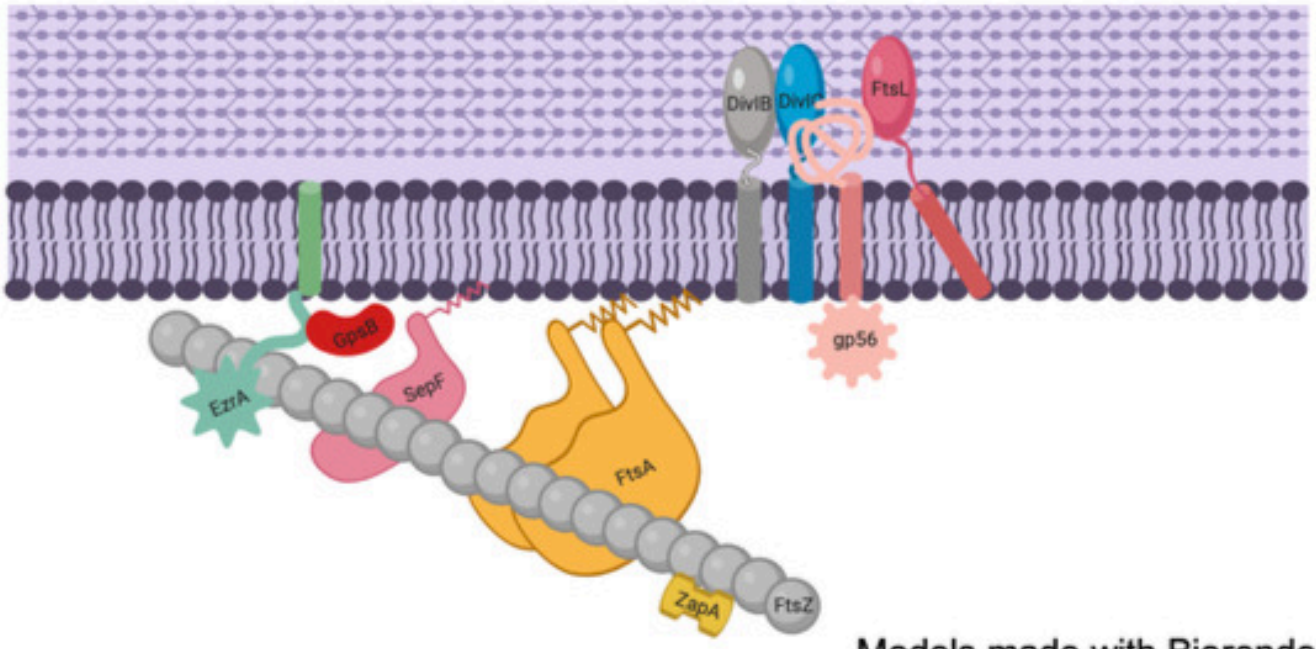

Models made with Biorender

TABLE 1. Bacterial strains used in this study.

Strain name	Species	Genotype	Source	Plasmid Intermediate
AIG184	*B. subtilis*	JH642 *yllB::P$_{spachy}$-yllB-ylxA-ftsL-pbpB cat*	A. Grossman	n/a
AIG23	*B. subtilis*	JH642 *ftsL::P$_{spac}$-ftsL-pbpB cat*	A. Grossman	n/a
BW121	*B. subtilis*	JH642 *ftsZ::spc xylA::tet thrC::P$_{xyl}$-ftsZ erm*	(55)	n/a
DPH102	*B. subtilis*	JH642 *amyE::P$_{spac}$-ORF56 cat*	This study	pDH83
DPH105	*B. subtilis*	JH642 *divIB::cat*	This study	n/a
DPH1108	*B. subtilis*	DPH579 pPW19	This study	n/a
DPH111	*B. subtilis*	PL847 *amyE::Pspac-ORF56 cat*	This study	n/a
DPH1119	*B. subtilis*	AIG23 *amyE::P$_{xyl}$-gfp-ORF56 cat::spc*	This study	n/a
DPH1121	*B. subtilis*	AIG184 *amyE::P$_{xyl}$-gfp-ORF56 cat::spc*	This study	n/a
DPH1152	*B. subtilis*	DPH648 *thrC::P$_{xyl}$-ORF56 erm*	This study	n/a
DPH162	*B. subtilis*	DPH50 *cat::spc*	This study	n/a
DPH170	*B. subtilis*	JH642 *amyE::P$_{xyl}$-gfp-ORF56 Δ65 cat*	This study	pDH91
DPH175	*B. subtilis*	JH642 *amyE::P$_{spac}$-ORF56 Δ65 cat*	This study	pDH92
DPH176	*B. subtilis*	JH642 pAP1	This study	n/a
DPH177	*B. subtilis*	DPH105 *amyE::P$_{xyl}$-gfp-ORF56 cat::spc*	This study	n/a
DPH2	*B. subtilis*	JH642 pPW19	This study	n/a
DPH3	*B. subtilis*	JH642 pAP6	This study	n/a
DPH302	*B. subtilis*	PL1237 *amyE::P$_{xyl}$-gfp-ORF56 cat*	This study	n/a
DPH324	*B. subtilis*	JH642 *amyE::P$_{spac}$-gfp-ORF56 cat*	This study	pDH112
DPH340	*B. subtilis*	JH642 *amyE::P$_{xyl}$-gfp-pbpB cat*	This study	pDH120
DPH371	*B. subtilis*	PL1201 *amyE::P$_{spac}$-ORF56 cat*	This study	n/a
DPH380	*B. subtilis*	JH642 *amyE::P$_{xyl}$-gfp-ftsW cat*	This study	pDH116
DPH387	*B. subtilis*	DPH380 *cat::spc*	This study	n/a
DPH400	*B. subtilis*	DPH340 *cat::spc*	This study	n/a
DPH408	*B. subtilis*	DPH387 pPW19	This study	n/a
DPH409	*B. subtilis*	DPH387 pAP6	This study	n/a
DPH414	*B. subtilis*	DPH400 pPW19	This study	n/a

DPH415	*B. subtilis*	DPH400 pAP6	This study	n/a
DPH462	*B. subtilis*	JH642 *thrC::P$_{xyl}$-ORF56 erm*	This study	pDH80
DPH50	*B. subtilis*	JH642 *amyE::P$_{xyl}$-gfp-ORF56 cat*	This study	pDH81
DPH503	*B. subtilis*	PL1269 *amyE::P$_{xyl}$-gfp-ORF56 cat::spc*	This study	n/a
DPH504	*B. subtilis*	BW121 *amyE::P$_{spac}$-gfp-ORF56 cat*	This study	n/a
DPH55	*B. subtilis*	PL867 *amyE::P$_{xyl}$-gfp-ORF56 cat*	This study	n/a
DPH576	*B. subtilis*	JH642 *amyE::P$_{xyl}$-gfp-ftsL cat*	This study	pDH138
DPH579	*B. subtilis*	DPH576 *cat::spc*	This study	n/a
DPH584	*B. subtilis*	DPH579 pAP6	This study	n/a
DPH602	*B. subtilis*	JH642 *amyE::P$_{xyl}$-gfp-divIC cat*	This study	pDH142
DPH614	*B. subtilis*	DPH602 *cat::spc*	This study	n/a
DPH617	*B. subtilis*	DPH614 pPW19	This study	n/a
DPH618	*B. subtilis*	DPH614 pAP6	This study	n/a
DPH632	*B. subtilis*	JH642 *amyE::divIC cat*	This study	n/a
DPH648	*B. subtilis*	DPH632 *cat::spc*	This study	n/a
DPH660	*B. subtilis*	DPH648 pPW19	This study	n/a
DPH661	*B. subtilis*	DPH648 pAP6	This study	n/a
DPH79	*B. subtilis*	JH642 *thrC::P$_{spac}$-gfp-divIB erm*	This study	n/a
DPH97	*B. subtilis*	DPH79 *amyE::Pspac-ORF56 cat*	This study	n/a
JH642	*B. subtilis*	*trpC2 pheA1*	(46)	n/a
KU608	*B. subtilis*	168 *trpC2 metC85::* Tn*917 divIB::cat*	(56)	n/a
PL1074	*B. subtilis*	JH642 *ftsAZ::P$_{spac}$-ftsAZ cat*	This study	pPL101
PL108	*B. subtilis*	PY79 *amyE::divIC cat*	(57)	n/a
PL1119	*B. subtilis*	JH642 *thrC::P$_{xyl}$-ftsZ erm*	This study	pPL104/pPL106
PL1201	*B. subtilis*	PY79 *divIVA::P$_{xyl}$-divIVA-gfp neo*	F. Gueiros-Filho	n/a
PL1237	*B. subtilis*	JH642 *divIC::P$_{spac}$-divIC erm*	This study	pDUG1
PL1269	*B. subtilis*	PL1074 *thrC::P$_{xyl}$-ftsZ erm*	This study	n/a
PL847	*B. subtilis*	JH642 *ezrA::ezrA-gfp spc*	(54)	n/a
PL867	*B. subtilis*	JH642 *ezrA::spc*	(54)	n/a

SU633	*B. subtilis*	168 *trpC2 thrC::*P_{spac}*-gfp-divIB erm*	E. Harry	n/a
AG1111	*E. coli*	MC1061 *F′ lacI*^{q} *lacZ* M15 Tn*10*	(47)	n/a
DHM1	*E. coli*	*F*$^{-}$ *cya*$^{-}$ *854 recA1 endA1 gyrA96 thi1 hsdR17 spoT1 rfbD1 glnV44(AS)*	(35)	n/a
DPH1164	*E. coli*	DHM1 pDH183 pDH186	This study	n/a
DPH1165	*E. coli*	DHM1 pDH183 pDH187	This study	n/a
DPH1166	*E. coli*	DHM1 pDH183 pDH188	This study	n/a
DPH1167	*E. coli*	DHM1 pDH183 pDH189	This study	n/a
DPH1183	*E. coli*	DHM1 pDH183 pKT25	This study	n/a

TABLE 2. Plasmids used in this study.

Plasmid name	Description	Oligos used (F/R)	Source
pAG58	pSI-1-/pJH101-derivative with IPTG-inducible P_{spac} for targeted integration of choice	n/a	(58)
pAP1	pPW19-*ORF58-ORF57-ORF56*	n/a	(18)
pAP6	pPW19-*ORF56*	n/a	(18)
pDH112	pDR67-*gfp-ORF56*	oDH306/148	This study
pDH116	pEA18-*ftsW*	oDH252/253	This study
pDH120	pEA18-*pbpB*	oDH262/263	This study
pDH138	pEA18-*ftsL*	oDH292/293	This study
pDH142	pEA18-*divIC*	oDH294/295	This study
pDH183	pUT18C-*ORF56*	oDH439/440	This study
pDH186	pKT25-*ftsL*	oDH432/434	This study
pDH187	pKT25-*divIC*	oDH435/437	This study
pDH188	pKT25-*ORF56*	oDH438/440	This study
pDH189	pKT25-*ORF56* Δ65	oDH438/440	This study
pDH80	pRDC19-*ORF56*	oDH149/148	This study
pDH81	pEA18-*ORF56*	oDH147/148	This study
pDH83	pDR67-*ORF56*	oDH149/148	This study
pDH89	pPW19-*ORF56 Δ65*	n/a	This study
pDH91	pEA18-*ORF56* Δ65	oDH147/148	This study
pDH92	pDR67-*ORF56 Δ65*	oDH149/157	This study
pDR67	pAG58-derivative integrative to *amyE* locus with IPTG-inductible P_{spac}	n/a	(47)
pDUG1	pRS14-*divIC* $_{5'-3'}$	*divIC* -5'/3'	This study
pEA18	pRDC18-derivative with *spoVG* RBS followed by *gfp* and in-frame *Not* I site	n/a	(59)
pJL62	pJH101-derivative for conversion of Cm^r $Spec^s$ strains to Cm^s $Spec^r$	n/a	(51)
pKT25	pSU40-derivative for in-frame 3'-end fusions to *cyaA* for BACTH analysis	n/a	(35)
pPL101	pAG58-*ftsA* $_{5'-3'}$	*ftsA* -5'/3'	This study
pPL104	pUC19-*ftsZ*	*ftsZ* -F4/R1	This study
pPL106	pRDC19-*ftsZ*	n/a	This study

pPW19	pSI-1-derivative with pUB110 origin with IPTG-inducible P_{spac}	n/a	(60)
pRDC18	pRDC9-/pDG1662-derivative integrative to *amyE* locus with xylose-inducible P_{xyl}	n/a	F. Arigoni
pRDC19	pRDC9-/pDG1664-derivative integrative to *thrC* locus with xylose-inducible P_{xyl}	n/a	F. Arigoni
pRS14	pAG58-derivative with *erm* cassette in place of original *cat* cassette	n/a	A. Grossman
pUC19	Standard cloning vector	n/a	(61)
pUT18C	pUC19-derivative for in-frame 3'-end fusions to *cyaA* for BACTH analysis	n/a	(35)

TABLE 3. Oligonucleotides used in this study.

Oligo name	Sequence	Target	Restriction site
divIC -3'	gatcgcatgctgcactaagggaagatgtttgg	*divIC*	*Sph* I
divIC -5'	gatcaagcttcataagaacgaccatcacacgg	*divIC*	*Hin* dIII
ftsA -3'	gatcgcatgcgaatttctttattttcactgg	*ftsA*	*Sph* I
ftsA -5'	gatcaagcttgttccgcaaataatagaatag	*ftsA*	*Hin* dIII
ftsZ -F4	gatcgctagcctattaagcatgttttgggaatag	*ftsZ*	*Hin* dIII (blunt)
ftsZ -R1	gatcggatcccgattttgtcctttacattagc	*ftsZ*	*Bam* HI
oDH147	gatcgcggccgctttaaatatacagatcgttcagtacgtcaatacattg	*ORF56*	*Not* I
oDH148	gatcggatcctcagttacgagcggcttcctg	*ORF56*	*Bam* HI
oDH149	gatcaagcttacaggggaatatacatatgtttaaatatacagatcgttcagtacgtcaatac	*ORF56*	*Hin* dIII
oDH157	gatcgcatgctcagttacgagcggcttc	*ORF56*	*Sph* I
oDH252	gatcgcggccgcttaaaaaaaatgctaaaatcttatgattactcactgatattcg	*ftsW*	*Not* I
oDH253	gatcggatccccctgtacacacttgttttttacagataaacag	*ftsW*	*Bam* HI
oDH262	gatagcggccgcattcaaatgccaaaaaagaataaatttatgaatagag	*pbpB*	*Not* I
oDH263	gataggatcccataacgacggctttcttttttaatcagg	*pbpB*	*Bam* HI
oDH292	ctaagcggccgcagcaatttagcttaccaacc	*ftsL*	*Not* I
oDH293	gattggatccggcatttgaatcattcctgtatg	*ftsL*	*Bam* HI
oDH294	ctaagcggccgcaatttttccagggaacgaac	*divIC*	*Not* I
oDH295	gattggatccgtgtcaacaaggctacttg	*divIC*	*Bam* HI
oDH306	gattaagcttgggaaaaggtggtgaactactatg	RBS_{spoVG} -*gfp*	*Hin* dIII
oDH432	tgtactgcagggagcaatttagcttaccaaccagagaaacag	*ftsL*	*Pst* I
oDH434	taaccccgggtcattcctgtatgtttttcacttttttatctttaaattcaag	*ftsL*	*Bam* HI
oDH435	cgtactgcagggaatttttccagggaacgaacgataactg	*divIC*	*Pst* I
oDH437	cctccccgggctacttgctcttcttctccacattgaagataacttctc	*divIC*	*Bam* HI
oDH438	tctgctgcagggtttaaatatacagatcgttcagtacgtcaatacattgaaaga	*ORF56*	*Pst* I
oDH439	gccactgcaggtttaaatatacagatcgttcagtacgtcaatacattgaaaga	*ORF56*	*Pst* I
oDH440	atcgcccgggtcagttacgagcggcttcctga	*ORF56*	*Bam* HI